Impact of Transmitter Positioning Uncertainty on RSS-based Visible Light Positioning Accuracy

Neha Chaudhary[1, 2], Luis Nero Alves[1, 2], Zabih Ghassemlooy[3]
[1]Instituto de Telecomunicações, Aveiro Portugal.
[2]University of Aveiro, Aveiro Portugal.
[3]Optical Comm. Research Group, Northumbria University, Newcastle-upon-Tyne, UK.
neha.chaudhary@ua.pt, nero@ua.pt, z.ghassemlooy@northumbria.ac.uk.

***Abstract*— This paper presents simulation-based results of the impact of transmitter (Tx) position uncertainty on the accuracy of the received signal strength (RSS)-based visible light positioning (VLP) system considering multipath reflections. RSS-based algorithms are constrained by several factors, most notably due to multipath channel characteristics and set-up uncertainties. A study on the impact of Tx uncertainties on positioning error performance is described. Simulation results show that, positioning accuracy can be severely compromised for positioning systems with a small number of Txs. We also show that higher lighting uniformity does not necessarily imply improved positioning performance. Furthermore, the error dependence on Tx's position uncertainty reduces with increasing the number of Txs.**

Keywords—VLC, OCC, CNN, ITS, visible light, camera, car, Driver, Image Processing.

I INTRODUCTION

The introduction of light emitting diodes (LEDs) has not merely developed the lighting world due to its tremendous advantages, such as high energy efficiency and longer lifetime compared with the conventional lighting bulbs, it has also opened up new applications. The emitted light signal can be modulated and hence, can transmit data, which is also known as visible light communications [1]. Visible light positioning (VLP) is another promising application of visible light where the location of the receiver (Rx) is estimated by the light-based access points [2-4]. VLP systems can employ a photodiode (PD) and/or camera as the Rx, where the latter reduces the complexity of the Rx [5]. There are different conventional approaches that can be used for position estimation, such as, received signal strength (RSS), angle-of-arrival, time-of-arrival where the distance or the angle between the transmitter (Tx) and the Rx is computed. In RSS, the optical signal at the Rx should be interference-free in order to estimate the distance accurately [6-9]. Performance analysis for these methods often relies on line of sight (LoS) channel conditions, which underestimate the achievable error bounds. More realistic models involving non-line of sight (NLoS) channel conditions have been carried before [10].

Research works have emphasized the effect of (*i*) noise on positioning performance [11]; (*ii*) reflections from walls and objects within the transmission paths [10]; and (*iii*) LED power uncertainty [12]. In [12], the impact of LED output power uncertainty on the accuracy of the VLP system in a real-life scenario was studied. In [13], the impact of the Tx's orientation (i.e., the tilting angle) on the accuracy of the VLP system was analysed. Different estimation approaches can be utilized to estimate the positioning of the Rx. For instance, in [14], an RSS-based VLP positioning system was investigated by employing a new regression-based approach along with linear and nonlinear least square estimations. The results showed that, the positioning error (PE) is less than 0.6 m using the regression approach, which is very low when compared with the traditional approaches. However, the impact of Tx's position on positioning estimation has not been fully explored yet, which is the subject of this paper.

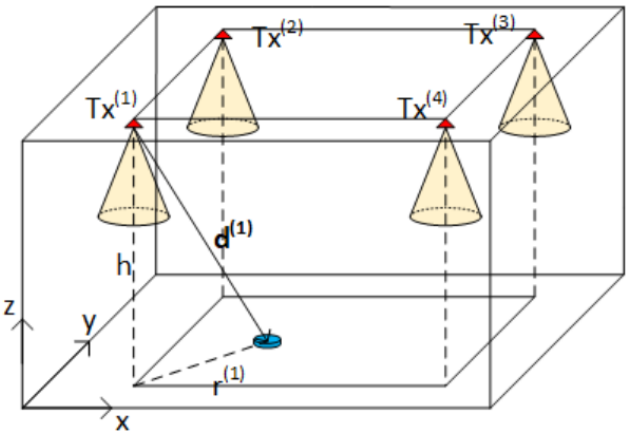

Fig. 1 System configuration.

In this work, we quantify the impact of Tx's position uncertainty under multipath reflections for the RSS-based VLP system. Lighting uniformity is an important parameter for well-lit indoor environments. Lighting uniformity, as well as positioning performance, are both related to the Tx's positions and the half power angles (HPA). Thus, our study investigates (i) how the lighting uniformity changes in the room for different HPAs and Tx's positions; and (ii) the impact of position uncertainties on the positioning accuracy (PA) considering the optimized positions from a lighting uniformity perspective.

The rest of the paper is organized as follows, Section II presents the system set-up, positioning algorithm, and different estimation approaches in detail. The impact of uniformity and different set-up uncertainties are presented in Section III. In Section IV, the impact of Tx's position uncertainty on error performance is discussed followed by the final concluding remarks in Section V.

II VLP SYSTEM MODELLING

2.1 System set-up

In this work, the VLP system consists of a single PD as the Rx and a number of LEDs as the Txs (in our case, 4, 9-

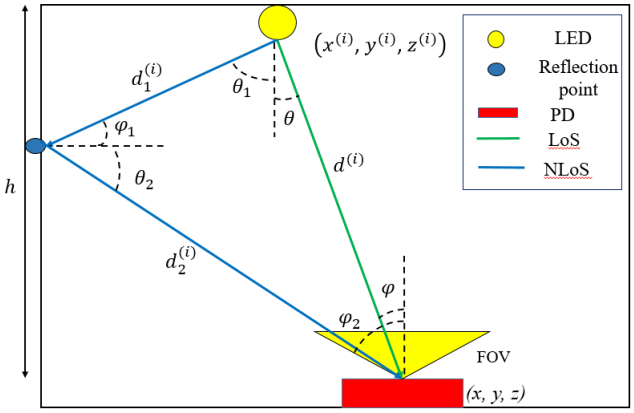

Fig. 2 The system model with a LED-based Tx and the PD-based Rx.

and 16-LED), which are installed on the ceiling of the room as shown in Fig. 1. In the algorithm, Txs are considered as the point sources, which are located at a height of 3 m from the ground level. The distance between the Txs depends on the lighting uniformity considerations, which are explained in the next section. In the proposed system. The PD has a field of view (FOV) and the detection area A_r of 70º and 10^{-4} m^2, respectively. Note, the area shown in the blue dashed line, see Fig. 1, is considered as the inner region while the rest is considered as the outer region.

The transmission paths between the Txs and the Rx considered are both the LoS and NLoS, see Fig. 2. Here, for the NLoS path we only consider the first-order reflection. However, higher-order reflections can be included but with not much improvement in the results at the cost of increased computation time. The received power $P_r^{(i)}$ from the i^{th} Tx can be expressed in terms of the power received from the LoS and NLoS paths, as given by:

$$P_{r(\text{total})}^{(i)} = P_{r(\text{LoS})}^{(i)} + P_{r(\text{NLoS})}^{(i)} \tag{1}$$

2.2 *RSS-based positioning*

The RSS method is used to obtain the estimated distance from the received power $P_r^{(i)}$ of the i^{th} Tx. Note, the transmit power P_t per Tx is assumed to be 1 W. The relation between $P_r^{(i)}$ and P_t for the LoS path can be expressed as [15]:

$$P_{r(\text{LoS})}^{(i)} = C_o P_t \frac{\cos^m(\theta)\cos(\varphi)}{\|\boldsymbol{d}^{(i)}\|^2} T_s(\varphi) g(\varphi), \tag{2}$$

where

$$C_o = \frac{m+1}{2\pi} \mathcal{R} A_r, \tag{3}$$

$$m = -\frac{\ln(2)}{ln(\cos(\text{HPA}))}, \tag{4}$$

where HPA is the half-power angle for the light source, θ is the irradiance angle from the Tx to the Rx, φ is the incident angle and $\mathcal{R}$ is the PD responsivity. $T_s(\varphi)$ and $g(\varphi)$ are the transmittance function and the concentrator gain of the Rx, respectively, which are considered to be unity. The distance $\boldsymbol{d}^{(i)}$ can be described as $\|\boldsymbol{d}^{(i)}\|^2 = r^{(i)^2} + h^2$ and therefore, we can calculate $r^{(i)^2}$ from (2) as given by:

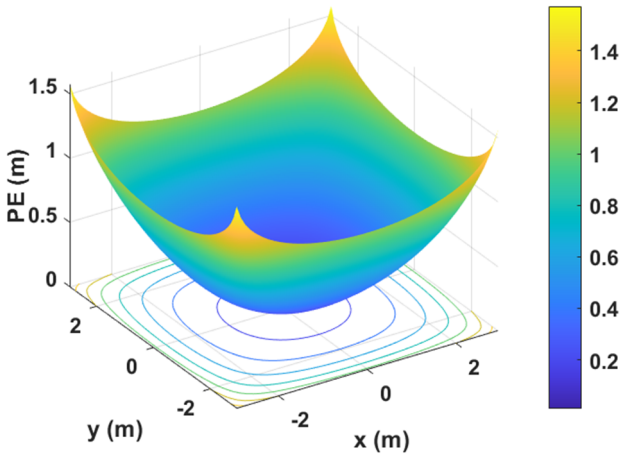

Fig. 3 The positioning error considering reflections with NLLS estimation.

$$\boldsymbol{r}^{(i)^2} = \left(\frac{P_t C_o h^{m+1}}{P_{r(\text{LoS})}^{(i)}}\right)^{\frac{2}{m+3}} - h^2, \tag{5}$$

where h is the vertical distance between the Tx and the Rx. In equation (5) the cosine terms are explicitly expressed in terms of the geometry of the set-up, as $h/\|d^{(i)}\|$.

The received power for the NLoS path (first-order reflection) can be expressed as [16]:

$$dP_{r(\text{NLoS})}^{(i)} = \rho C_o P_t dA \frac{\cos^m(\theta_1)\cos(\varphi_1)}{\pi\left(\|\boldsymbol{d}_1^{(i)}\|\|\boldsymbol{d}_2^{(i)}\|\right)^2} T_s(\varphi_2) \times g(\varphi_2)\cos(\theta_2)\cos(\varphi_2), \tag{6}$$

where $\boldsymbol{d}_1^{(i)}$ is the distance between the Tx and the reflective area, $\boldsymbol{d}_2^{(i)}$ is the distance between the reflective area, see Fig. 2, and the Rx and ρ is the reflectance factor depending on the material of the reflective surface. For NLoS, we integrate (6) over all the walls for each Tx, assuming a grid area with a resolution dA of 0.1 m.

2.3 *Estimation using nonlinear least squares*

The Rx coordinates (x, y) are related to the Tx coordinates $(x^{(i)}, y^{(i)})$ using the following equations:

$$\begin{cases} \left(x - x^{(1)}\right)^2 + \left(y - y^{(1)}\right)^2 = \boldsymbol{r}^{(1)^2} \\ \left(x - x^{(2)}\right)^2 + \left(y - y^{(2)}\right)^2 = \boldsymbol{r}^{(2)^2} \\ \vdots \\ \left(x - x^{(n)}\right)^2 + \left(y - y^{(n)}\right)^2 = \boldsymbol{r}^{(n)^2} \end{cases}, \tag{7}$$

where n is the number of Txs. Nonlinear least square (NLLS) estimation method is used for position estimation, where the solution can be estimated by obtaining $\tilde{X} = [\tilde{x}, \tilde{y}]$ that minimizes the cost function is given by [11]:

$$\tilde{Q} = \sum_i \left(\sqrt{(x - x^{(i)})^2 + (y - y^{(i)})^2} - \boldsymbol{r}^{(i)}\right)^2. \tag{8}$$

An iterative procedure is utilized to estimate $\tilde{X}$ by employing the trust-region reflective algorithm [17]. In this algorithm, first, an estimate is introduced as $\tilde{X}_0$, followed by computing the corresponding cost function $\tilde{Q}_0$. Next, several points in the neighbourhood of $\tilde{X}_0$ are replaced in (8), and the

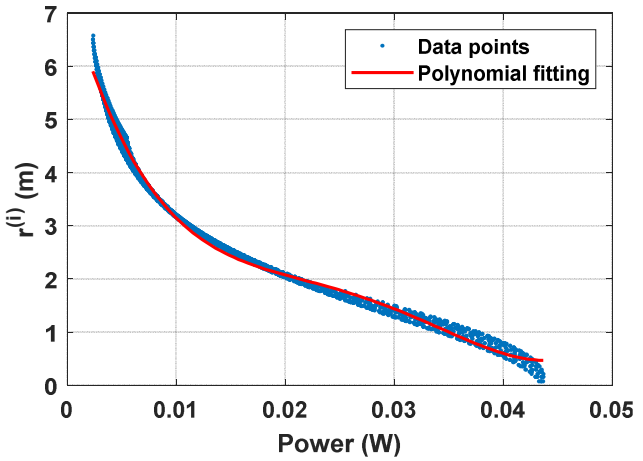

Fig. 4 Estimation using polynomial fitting method.

one that minimizes the cost $\tilde{Q}_1$ is selected as $\tilde{X}_1$. The Rx coordinates $\tilde{X}$ will eventually be obtained following several iterative steps to ensure that $\tilde{Q}$ converges. In the proposed system, the initial value for $\tilde{X}_0$ is estimated using a linear least square.

Fig. 3 shows an example of the PE due to the nonlinear least square estimation for the system with 4-Tx. We can see that, the maximum PE is around 1.57 m, which is high and is due to multipath reflections. When considering multipath reflections, the power-distance LoS model in (5) is not accurate for the NLoS case. This introduces a large bias in the estimation process which cannot be recovered using nonlinear least-squares method alone.

2.4 Polynomial regression

This approach analyses the relationships between a dependent variable (outcome) and one or several independent variables (features). There are different types of regression approaches as outlined in [18]. Here, the polynomial regression is adopted, where the relationship between the features and the outcome is described as an n^{th} degree polynomial. In this particular case, for the i^{th} Tx, the relation between $d^{(i)}$ and $P_{r(\text{total})}^{(i)}$ is given as:

$$d^{(i)} = a_0 + a_1 P_{r(\text{total})}^{(i)} + \cdots + a_n \left(P_{r(\text{total})}^{(i)}\right)^n, \quad (9)$$

where a_k, are the polynomial coefficients. Using all the data points extracted from the channel simulation we estimated the best polynomial fitting in the linear squares sense, depicted in Fig. 4. The value of R^2 (coefficient of determination) was investigated for different orders, the best-fitted solution exhibited, and R^2 of 0.8942 for a 4$^{\text{th}}$ order polynomial.

Fig. 5 illustrates the cumulative distribution function (CDF) against the PE for non-linear least square with and without polynomial regression. Assuming that PE is a random variable (it may depend on uncertainties (for instance, Tx's position uncertainties, σ, as it will be described in section 3.1), noise, or even the estimation process itself), it is logical to use the standard statistical analyses definition for the probability distribution function (PDF) and CDF. In this case, the PDF and CDF are constructed based on the spatial distribution of PE within the room. The PDF, denoted by f_{PE} is given by,

$$f_{\text{PE}}(x) = \lim_{\substack{N\to\infty \\ \varepsilon\to 0}} \frac{\#\text{PE}(|PE - x| \le \varepsilon)}{N}, \quad (10)$$

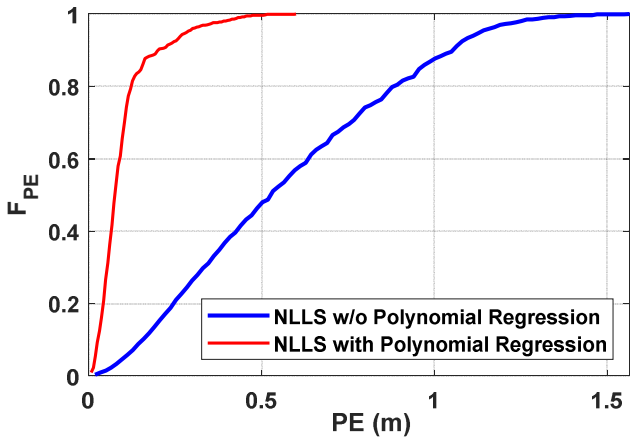

Fig. 5 CDF of the errors measured by NLLS and NLLS with polynomial regression estimation.

where N is the number of samples and ε defines an error interval centered around x. The cardinal operator # represents the counting of occurrences were |PE-x|<ε. The limiting process is naturally implied by the discrete nature of the simulation. The CDF, F_{PE} is then obtained using,

$$F_{\text{PE}}(x) = \int_0^x f_{\text{PE}}(x)dx. \quad (11)$$

As shown in Fig. 5, there is a noticeable improvement in the accuracy when using non-linear least squares combined with polynomial regression for power-distance modeling. The maximum PE is 0.6 m with polynomial regression as compared with the non-linear least square estimation that achieves the maximum PE of 1.57 m. As depicted in Fig. 5, the polynomial regression allows to improve PA without involving high complexity algorithms.

III Set-up Uncertainties

3.1 Uncertainties of the Tx's position

Investigating the uncertainties of the Tx's position introduces a challenge in simulation. That is, to study uncertainties we must use random Tx positions, which implies that, for each iteration we must re-simulate the channel, which leads to the increased simulation time. In order to fully understand the problem, we have devised two approaches (i) a direct process; and (ii) a reverse process. In the former, we assume that the channel is re-simulated and the impact of uncertainties is measured following a 500 random iterations. In the latter, we assume that the channel is fixed for a set of ideal positions and the uncertainties are fed into the system using (7). Selecting just one equation from (7), for the direct process we have at each step the following:

$$(R(1) - XT)^2 + (R(2) - YT)^2 = f_R(XT + dX, YT + dY), \quad (12)$$

where $R(1)$ and $R(2)$ are the coordinates of the Rx, XT, and YT are the coordinates of the Tx, and dX and dY express the uncertainty at the Tx coordinates. Both dX and dY are assumed to be Gaussian variables with $N(0, \sigma^2)$ probability density function. As stated in (12), at each iteration the channel needs to be re-simulated in order to extract the distance measure.

The reverse process does not require the channel re-simulation at each iteration as given by:

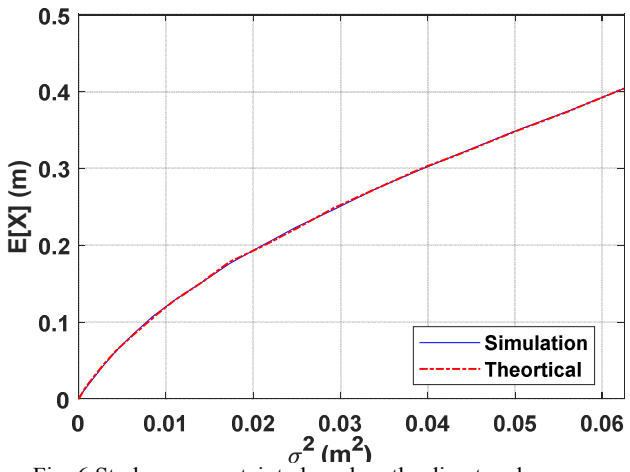

Fig. 6 Study on uncertainty based on the direct and reverse processes.

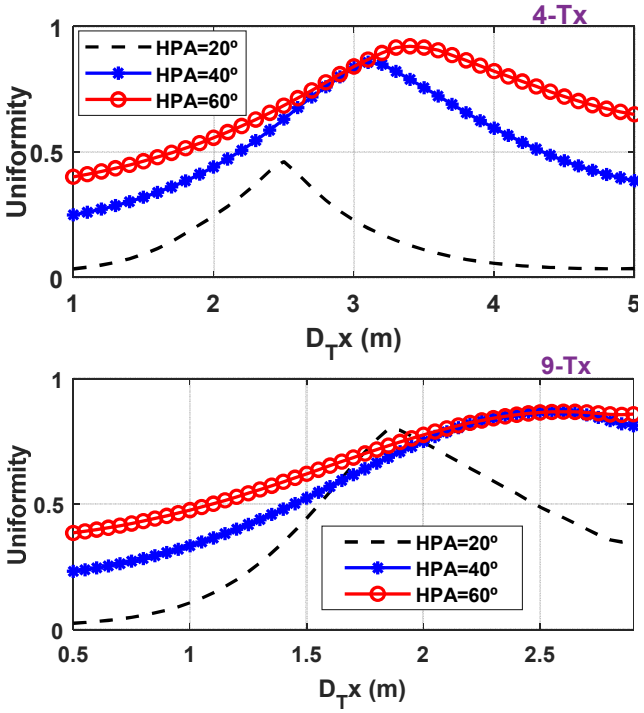

Fig. 7 Comparison of uniformity for different HPA and distance between the Txs in case of: (a) 4-Tx and (b) 9-Tx.

$$(R(1) - XT - dX)^2 + (R(2) - YT - dY)^2 = f_R(XT, YT). \quad (13)$$

Subtracting (12) and (13) and extracting the mathematical expectation of both sides gives:

$$E[dX^2 + dY^2 - 2dX(R(1) - XT) - 2dY(R(2) - YT)] = 2\sigma^2]. \quad (14)$$

Equation (14) states that, the reverse process has an expectation, which is given by:

$$U_r(\sigma_r) = 2{\sigma_r}^2. \quad (15)$$

Performing the same analysis for the direct process we have:

$$U_d(\sigma_d) = E[fR(XT, YT) - fR(XT + dX, YT + dY)]. \quad (16)$$

Note, U_d can be estimated through numerical simulation. Closed-form expressions are not a viable option due to the fact that, the channel itself has no closed-form expression for the NLoS case. Following mathematical simulation, and assuming that the Rx is positioned at the center of the room and a grid representing the Tx's positions, we have obtained the values for $U_d(\sigma)$ for different values of σ, see Fig. 6. Note, the two processes are equivalent provided the generated uncertainties are equal for certain values of σ_r and σ_d. This indicates that, the reverse process uncertainty can be generated from the knowledge of the direct process using the following:

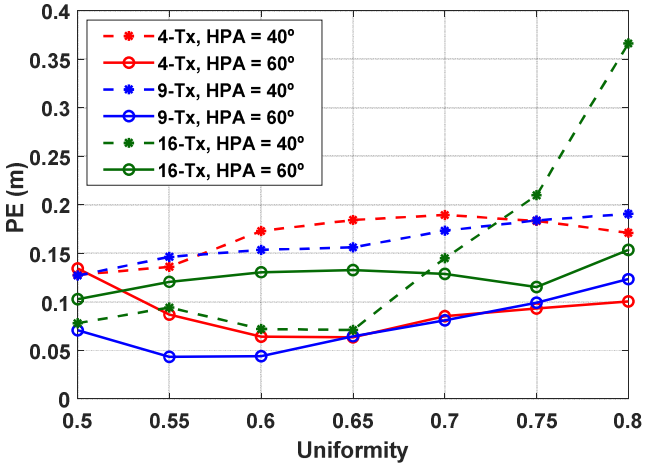

Fig. 8 Comparison of positioning error for different Txs and uniformity.

$$\sigma_r^2 = \frac{U_d(\sigma_d)}{2}. \quad (17)$$

3.2 *Lighting uniformity*

Lighting levels normally depend on the condition of the environments [19]. In indoor environments such as offices uniform distribution of the light with the sufficient level essential. In such scenarios, the lighting uniformity U is:

$$U = \frac{P_{r_{\min}}}{P_{r_{\max}}}, \quad (18)$$

where $P_{r_{\min}}$ and $P_{r_{\max}}$ are the minimum and maximum detected optical power levels at the illuminated target, respectively. Uniformity depends on the three factors related to the Txs, i.e., HPA, the distance between the Txs, and the number of Txs. Fig. 7 shows the uniformity of lighting as a function of the number of Txs (i.e., 4 and 9) and for a range of HPA. As can be seen, a higher number of Txs offer better uniformity. The maximum uniformities are at distances of 3.4 and 2.6 m for HPA of 60º for 4- and 9-Tx, respectively. Note that, the same factors, which affect lighting uniformity, also impact the PA. It is normally assumed that higher uniformity translates itself into improved PA. As our study shows, this is not a general rule, in fact, HPA seems to have a more pronounced impact on the PA than the uniformity.

3.2.1 *PE dependence on lighting uniformity*

In this subsection, we further characterize the PEs for different HPA and uniformity. For this, we vary the uniformity between 0.5 and 0.8 in steps of 0.05 and for HPA of 40º and 60º. This is accomplished by setting the distance between the Txs according to the results of Fig. 7. For each of this set of conditions, we estimate the PE using nonlinear least squares with the polynomial regression power-distance model, as before. Fig. 8 illustrates the PE for different uniformity for 4-, 9- and 16-Tx. It can be seen. that PE depends on both

Table I. The optimized values for all Txs case.

Number of Txs	Distance between Txs (m)	Uniformity	HPA (°)
4	2.4	0.65	60
9	1.3	0.55	60
16	1.34	0.65	40

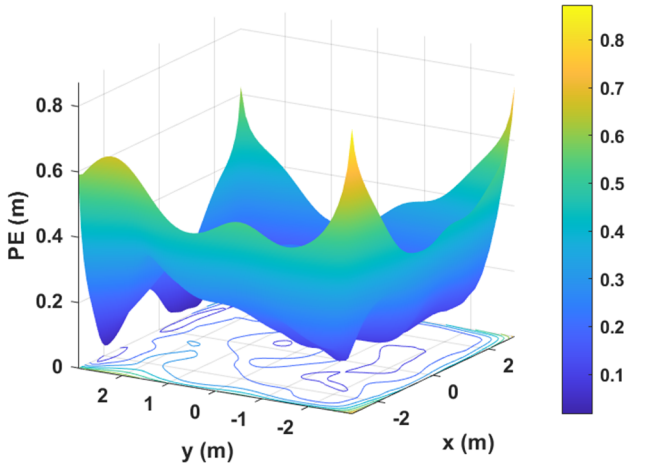

Fig. 9 Positioning error considering reflections and uncertainty using NLLS with polynomial regression.

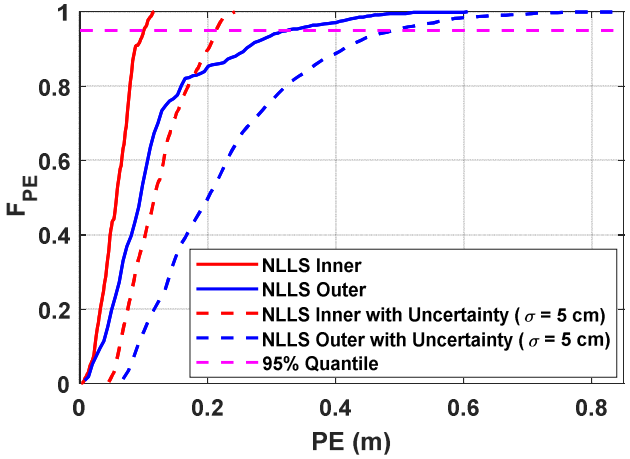

Fig. 10 Comparison of the CDF of positioning errors.

uniformity and HPA. For instance, for 4-Tx, the minimum PE is achieved for HPA of 60º and with uniformity equal to 0.65, while, in the case of 9-Tx, the minimum PE is attained with HPA of 60º and uniformity of 0.55. For the 16-Tx case, the minimum PE is achieved with an HPA of 40º and uniformity of 0.65. Results in Fig. 8 show that: (*i*) low to moderate lighting uniformity can support low PE; and (*ii*) there is an optimum value for the number of Txs and the associated HPA, which do not match the optimum lighting uniformity conditions. Under the simulated conditions, table I collects the optimum values for the distance between the Tx, HPA, and uniformity based on the lowest PE.

3.3 Performance with Tx's position uncertainties

This section investigates the impact of Tx's position uncertainties on PE. To simulate the effect of Tx's position uncertainty, the ideal positions of the Txs are added with a random displacement vector *(dX, dY)* as described in section 3.1. The simulation follows the reverse method described in section 3.1, using the adjusted variance values given by (17). Fig. 9 shows the PE for a single random iteration using NLLS

Table II. The default value of the system's parameters.

Parameter	Value
Room size	$6 \times 6 \times 3$ m^3
Area of PD	10^{-4} m^2
Responsivity of PD	1 A/W
Field of view (FOV)	75º
Transmitted power	1 W
Reflection coefficient	0.7
Tx elevation	-90º
Tx azimuth	0º
Rx elevation	90º
Rx azimuth	0º

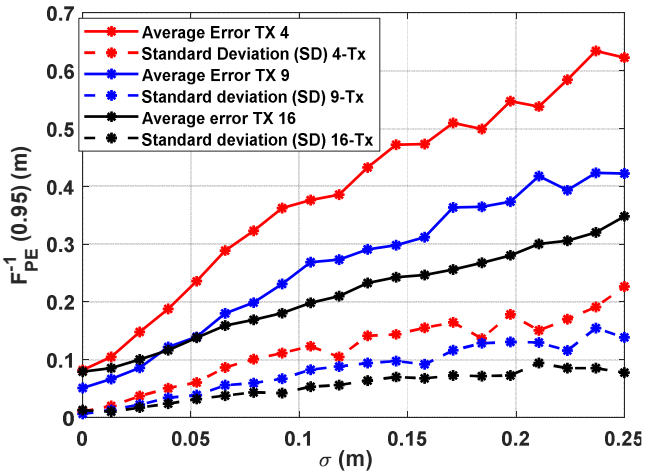

Fig. 11 Comparison of positioning error for different Txs and σ.

with polynomial regression. Comparing with Fig. 3, the effects of Tx's uncertainty is noticeable. The effect of multiple iterations is difficult to analyse using 3-dimensional surface plots of the PE. CDF plots of PE distribution are more adequate for this matter. Fig. 10 shows an example of F_{PE} obtained after averaging 100 random iterations of the Tx's positions with σ of 5 cm, for the case of 4-Tx. Fig. 10 shows two error measures, considering the inner and outer regions of the room as depicted in Fig. 1. The Tx's uncertainty raises the error, with a more pronounced effect on the outer region of the room (close to walls and corners). Fig. 10 also shows the 95% quantile, showing how large is PE for 95% of the cases. Here the quantile function is taken as the inverse function of F_{PE},

$$x = {F_{\mathrm{PE}}}^{-1}(p) \tag{18}$$

where p represents the quantile of interest and x is the error measure. In Fig. 10, the 95% quantile is depicted in an average sense, for the case of the uncertainty in Tx's positions.

IV IMPACT OF TX'S POSITION UNCERTAINTY ON ERROR PERFORMANCE

The simulation setup is composed of a room of dimension $6 \times 6 \times 3$ m^3 and LEDs, which are assumed to be the same and modeled as pointwise Lambertian sources with the order m depending on the value of HPA, see (2). Here, we have considered three different cases of 4-LEDs, 9-LEDs, and 16-LEDs, which are placed in a square grid on the ceiling plane. The Tx spacing within the grid is set according to light

uniformity requirements as summarized in table I. The Rx is placed on the ground plane. The grid resolution is fixed at 1 cm for all simulation purposes, which implies that the PD can be placed at 3600 different locations. All the default parameters for the simulation are shown in table II. The effect of Tx's uncertainty on PE followed a similar procedure as before, with 100 random iterations for each σ value. The 95% quantile is used as PE performance metric, considering both, its average and standard deviation, over the 100 random iterations.

Fig. 11 depicts the average and standard deviation of the 95% quantile of PE as a function of σ for 4-, 9- and 16-Tx. Fig. 11 shows that the effect of Tx's uncertainty, σ, traduces in an increasing error dependence, which is more pronounced for set-ups with a lower number of Txs. The spreading of the error, represented by the standard deviation of the error quantile, also shows an increasing trend with σ, being more pronounced for the 4-Tx case. Fig. 11 suggests that increasing the number of Txs proves effective in terms of reducing the error dependence on Tx's position uncertainty.

V CONCLUSIONS

This paper presented results on the influence of Tx's position uncertainty in the performance of visible light positioning systems based on RSS. Achieved results showed that light uniformity and Tx's HPA are crucial design parameters. The selection of the Tx's HPA as well as the optimum distance between Txs has to be considered carefully. Moreover, optimum uniformity and optimum error performance are not met for the same conditions, implying necessary design trade-offs. For square grid Tx placement, the number of Txs can be explored as an added variable for the optimization of both light uniformity and error performance, as it allows the reduction of HPA for smaller distances between Txs.

ACKNOWLEDGMENT

This work is supported by H2020/MSCA-ITN funding program under the framework of European Training Network on Visible Light Based Interoperability and Networking, project (VisIoN) grant agreement no 764461.

REFERENCES

[1] A. Jovicic, J. Li, and T. Richardson, "Visible light communication: opportunities, challenges and the path to market," IEEE Communications

[2] J. Luo, L. Fan, and H. Li, "Indoor Positioning Systems Based on Visible Light Communication: State of the Art," IEEE Commun. Surveys Tuts., vol. 19, no. 4, pp. 2871-2893, 2017.

[3] T. H. Do and M. Yoo, "An in-depth survey of visible light communication based positioning systems," Sensors (Basel), vol. 16, no. 5, May 2016.

[4] N. Chaudhary; L. N. Alves; Z. Ghassemlooy, " Current Trends on Visible Light Positioning Techniques", The 2nd West Asian Colloquium on Optical Wireless Communications (WACOWC2019), Apr 2019, Tehran, Iran. ffhal-02135266.

[5] M. Yoshino, S. Haruyama, and M. Nakagawa, "High-accuracy positioning system using visible light and image sensor,"in Proc. IEEE Radio Wireless Symp., 2008, pp. 439–442.

[6] S. H. Yang, D. R. Kim, H. S. Kim, Y. H. Son and S. K. Han., "Visible light based high accuracy indoor localization using the extinction ratio distributions of light signals," Microwave Opt. Technol. Lett. Vol. 55, no. 6, pp. 1385–1389, 2013.

[7] T. Nguyen and Y. M. Jang, "Highly Accurate Indoor Three-Dimensional Localization Technique in Visible Light Communication Systems," The Journal of Korea Information and Communications Society, vol. 38, no. 9, pp. 775-780, Sep. 2013.

[8] N. U. Hassan, A. Naeem, M. A. Pasha, T. Jadoon, and C. Yuen, 'Indoor positioning using visible led lights: A survey', ACM Comput. Surv. CSUR, vol. 48, no. 2, 2015.

[9] B. Lin, X. Tang, Z. Ghassemlooy, c. Lin and Y. Li, "Experimental demonstration of an indoor VLC positioning system based on OFDMA," IEEE Photonics Journ., vol. 9, no. 2, pp. 1–9, 2017.

[10] W. Gu, M. Aminikashani, P. Deng, and M. Kavehrad, "Impact of Multipath Reflections on the Performance of Indoor Visible Light Positioning Systems",. J. Lightwave Technol. vol. 34, pp. 2578–2587, 2016.

[11] F. I. K. Mousa, N. Almaadeed, K. Busawon, A. Bouridane, R. Binns and I. Elliott, "Indoor visible light communication localization system utilizing received signal strength indication technique and trilateration method", Opt. Eng. Vol. 57, no. 016107, 2018.

[12] D. Plets, S. Bastiaens, N. Stevens, L. Martens and W. Joseph, " Monte-Carlo Simulation of the Impact of LED Power Uncertainty on Visible Light Positioning Accuracy". in Proceedings of the 11th International Symposium on Communication Systems, Networks & Digital Signal Processing, CSNDSP 2018, Budapest, Hungary, 18–20 July 2018; pp. 1–6.

[13] D. Plets, S. Bastiaens, L. Martens, W. Joseph, "An analysis of the impact of LED tilt on visible light positioning accuracy", Electronics, 8 (4), 2019.

[14] S. Shawky, M. A. El-Shimy, Z. A. El-Sahn, M. R. Rizk and M. H. Aly, "Improved vlc-based indoor positioning system using a regression approach with conventional rss techniques", Wireless Communications and Mobile Computing Conference (IWCMC) 2017 13th International, 2017, pp. 904-909.

[15] N. Chaudhary, L. N. Alves and Z. Ghassemblooy, "Feasibility Study of Reverse Trilateration Strategy with a Single Tx for VLP," 2019 2nd West Asian Colloquium on Optical Wireless Communications (WACOWC), Tehran, Iran, 2019, pp. 121-126.

[16] Z. Ghassemlooy, W. Popoola and S. Rajbhandari, Optical Wireless Communications: System and Channel Modelling with MATLAB®, Second Edition, CRC Press, 2019.

[17] J. J. Mor and D. C. Sorensen, "Computing a trust region step," SIAM J.Sci. Statist. Comput., vol. 4, no. 3, pp. 553–572, 1983.

[18] J. L. Buchanan and P. R. Turner, Numerical Methods and Analysis, New York: McGraw-Hill, 1992.

[19] Y. Hu, M. R. Luo, Y. Yang, "A study on lighting uniformity for LED smart lighting system", Proc. 12th China Int. Forum Solid State Lighting (SSLCHINA). 2015: 127-130.